



Electrical Properties of Thermally Sprayed Ni- and Ni20Cr-Based Resistors

Maria Prudenziati and Magdalena Lassinantti Gualtieri

(Submitted September 15, 2007; in revised form November 12, 2007)

Five laboratories were asked to deposit Ni and Ni20Cr powders to obtain resistors; we studied their electrical properties in the temperature range 20–500 °C and interpreted the results in the light of their microstructure. Resistors sprayed from Ni powders consist of NiO_x “islands” embedded in a Ni matrix. The temperature dependence of resistance (TCR) is in perfect agreement with that of pure Ni, indicating that the matrix determines the electrical transport. Annealing at temperatures from 200 to 400 °C results in an irreversible decrease of resistance. A multiphase microstructure is observed in resistors prepared from 80Ni20Cr powders. The major phase in these resistors is a NiCr alloy but with a Ni:Cr ratio larger than 80:20. Minor amounts of metal oxides are also detected. The TCR in these samples spans from 180 ppm/°C to 2830 ppm/°C, and is attributed to different degree of oxidation and segregation of the metals in the alloy.

Keywords annealing, electrical conduction, nickel, NiCr, oxidation, thermal spray

1. Introduction

Thermal spray processes, such as Atmospheric Plasma Spray (APS) and High Velocity Oxy-Fuel (HVOF), allow the deposition of a wide variety of materials. A powder feedstock is delivered in a high temperature flame. The melted particles are propelled, in a plastic state as well as in a vapor state due to sublimation or evaporation of the original/reacted feedstock powder, by gas streams at very high speeds toward the substrate (Ref 1, 2). Impinging on the substrate, the particles condense and rapidly solidify to form so-called splats. Coatings are formed by the build-up of successive layers of splats giving rise to a lenticular structure. As a result, sprayed materials are characterized by a complex, anisotropic microstructure comprised of elongated brick-like lamellae separated by interlayer pores. In addition, secondary phases (e.g., interlayer or segregated oxides in the case of metallic coatings) and other (intralayer or interlayer) heterogeneities and defects are distributed in a complex way through the coating (Ref 3).

The main application of thermal spray technologies has been for the deposition of protective coatings against wear, heat, corrosion, and oxidation. In particular, Ni and its alloys (e.g., Ni20Cr, NiCrAlY, NiCoCrAlY) are widely used, e.g., for reclamation (re-work and repair of damaged

parts) and bond coats. Therefore, a myriad of investigations on the mechanical, tribological, and thermal properties of these coatings can be found in the literature. Recently, the interest is emerged in new applications of thermal spray metals for heaters (Ref 4–8) and sensors (Ref 3, 9, 10). In this perspective, the electrical properties (such as resistance and TCR) of thermally sprayed resistors as well as their reliability are important characteristics to be taken into account for the design and development of devices.

Unfortunately, electrical properties of thermal-sprayed metals have been sporadically addressed (Ref 3, 11–13). The main purposes of this article are to contribute to fill the gap in this subject and to investigate if electrical characterization may be a valuable means for the inspection of the microstructural features of the coatings.

We would remark here, however, that the details in microstructural differences among the types of metal layers and their linkage to processing parameters are out of the scope of this work (and it should be restricted by the unwillingness of some laboratories to provide sufficient information on the conditions of spray procedures). Therefore, we confined our analyses to the search for major differences in composition and microstructure to be related to differences in electrical properties of the various samples.

2. Experimental

2.1 Materials and Sample Preparation

Five different laboratories (hereafter designed with the letters F, P, R, S, Z) were asked to prepare, with their usual atmospheric plasma spray (APS) processes and equipments, meandering patterns from both Ni and Ni20Cr commercial powders. One series of HVOF-sprayed resistors was also prepared by one laboratory.

Maria Prudenziati and Magdalena Lassinantti Gualtieri, Dipartimento di Fisica, Università di Modena e Reggio Emilia, Via G. Campi 213/A, 41100 Modena, Italy. Contact e-mail: prudenziati.maria@unimore.it.

Each sample series will from now on be designated by a capital letter referring to the laboratory from where they came from, followed by the batch number (when more than one batch was prepared from the same lab) and the type of metal powder (e.g., P1-Ni20Cr refers to a sample from batch number one, prepared by laboratory P, and APS-sprayed Ni20Cr powder), whereas the designation S-Ni20Cr-HVOF refers to the series of resistors prepared in laboratory S, spraying Ni20Cr powder with the HVOF process. Table 1 reports, for each sample series, in batches of 10-12 samples, the commercial names of the powders and their size distribution together with length and width of the resistive pattern. Table 2 reports the composition of the powders, according to the certificate provided by the manufacturer or our analytical results.

The majority of the samples were prepared on steel coupons but also bronze was occasionally used for comparison (see Table 1). Figure 1 shows an in-plane and side view sketch of a typical sample. The metal coupons were mildly grit blasted with alumina grit (R_a in the range 2-4 μm) and subsequently coated with an adequate interface (not shown in Fig. 1) which serves to avoid corrosion/oxidation of the substrate as well as of the resistor (Ref 13). A first layer of alumina (ca. 100 μm thick) was sprayed on the metal coupon to electrically insulate the substrate. Subsequently, a meandering pattern (resistor) was formed by spraying through a metal mask. Eventually, a second alumina coating (ca. 70 μm thick) was sprayed on the entire sample (exception made on the resistor pads for electrical connections) which provided the crucial protection of the resistor to oxidation and contamination from the environment.

Table 1 Resistors prepared in various laboratories (see text for explanation of sample series codes)

Sample series	Metal powder/particle size, μm	Resistor width/length, mm
Z-Ni	Metco 56FNS/-45, +11	2/260
R-Ni	TAFa 1166 F/-53, +20	2/200
F-Ni	NA	2/260
S-Ni20Cr	Metco 43VF-NS/-45, +5	2/625
P1-Ni20Cr	Ni-106/-90, -10	1/233
P2-Ni20Cr	Ni-106/-90, -10	1/233
Z-Ni20Cr	Metco 43C-NS/-106, +45	2/215
R-Ni20Cr	Metco 43C-NS/-106, +45	...
S-Ni20Cr-HVOF	Metco 43VF-NS/-45, +5	2/621

The commercial powders and their size are reported, as well as the two-dimensional geometry of the mask used for the resistive pattern

Table 2 Chemical composition of powders (wt.%)

Powder	Ni	Co	Fe	T.A.O	Cr	Si	Note
Metco 56FNS	99.76	0.12	0.02	0.10			(a)
Tafa 1166 F	99.3			0.70	...		(a)
Metco 43C-NS	78.46		0.5	0.01	19.83	1.2	(a)
Metco 43VF-NS	79.15		0.5		18.77	1.09	(b)
Ni-106	81-79				19-21		(b)

(a) Analysis. (b) Certificate of the powder's manufacturer

2.2 Measuring and Analytical Method

The sample resistance at room temperature was measured with the four wires method (Philips Multimeter PM 2528). A rough estimation of the electrical resistivity (ρ) was calculated using the resistance and the geometrical parameters of the patterns, according to Ohm's law. Large uncertainties of the computed values were obtained due to the irregular geometry of the patterns, which exhibit large variation in thickness both along the pattern and across its width. The latter is demonstrated in Fig. 2 which shows a BSE image of a typical resistor in cross section. It is apparent that the irregular thickness of the resistor is the result of the roughness of both alumina coatings and the metal layer itself. In addition, the resistor has tapered edges.

Data for the temperature dependence of resistance were collected during self-heating of the samples, i.e., recording the values of flowing currents and the corresponding voltage drops across the resistor operating as a heater (Ref 8). Either d.c. current (for Ni20Cr-based

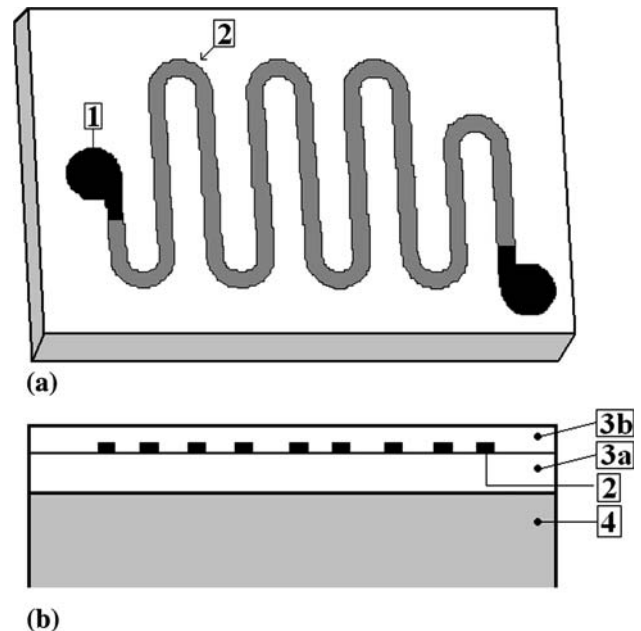


Fig. 1 In-plane (a) and side view (b) sketch of a sample, showing the contacts (1) connected by a metal meander (2). The meander is electrically insulated from the metallic support (4) by an alumina layer (3a). A second protective alumina layer is deposited on top of the meander (3b)

samples) and a.c. current (for Ni-based samples) was applied. The applied current was increased to heat the sample with a rate of approximately $6\text{ }^{\circ}\text{C min}^{-1}$. The temperature was measured with a thermocouple inserted in the metal substrate, just below the resistor center.

The temperature coefficient of resistance (TCR) was calculated according to:

$$TCR = \frac{(R - R_0)}{R_0(T - T_0)} \quad (\text{Eq 1})$$

where R_0 is the electrical resistance at a reference temperature T_0 .

To investigate the short-time and long-time stability of resistance at high temperatures, experiments were performed in which as-sprayed resistors were subjected to repeated temperature cycles and annealing processes. Each annealing was performed for a dwell time of 2 h at various temperatures. The resistance at room temperature was registered after each temperature cycle.

The phase composition of sprayed metals was determined with X-ray Powder Diffraction (XRPD) analyses, using a θ/θ diffractometer (PANalytical, Cu $K\alpha$ radiation) equipped with a RTMS detector. Data were collected in continuous mode with $1/2^{\circ}$ fixed divergence and antiscatter slits, 0.04 mrad soller slit on both the incident and secondary beam, fixed 5 mm RTMS slit, and Ni filter on the secondary beam. An integrated step scan of the RTMS

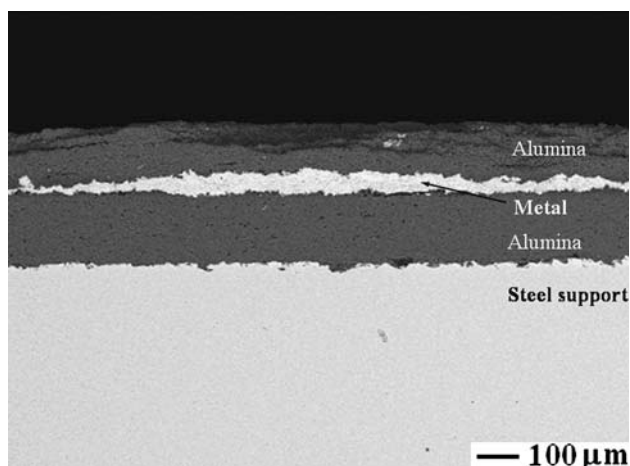


Fig. 2 BSE image of a resistor, in cross section, showing highly irregular thickness and tapered edges

detector of $0.0167273^{\circ} 2\theta$ was used with a high counting statistic (200 s/step).

Coating thickness, morphology, and microstructure were examined by Scanning Electron Microscopy (SEM), using a Philips XL-40 microscope equipped with a Everhart Thornley detector for secondary electrons (SED image), a solid-state detector for backscattered electron (BSD-images), and an energy dispersive X-ray fluorescence spectrometer (EDS). The EDS system includes an Oxford-SATW Si(Li) detector (detected elements with $Z \geq 6$) and the X-EDS Oxford INCA software. Samples for in-plane view were prepared by gentle polishing and subsequent cleaning in ethanol under ultra-sonification. Samples for cross view were embedded in epoxy resin prior to polishing and cleaning. The samples, mounted on aluminum stubs, were coated with a thin layer of gold or carbon (ca. 10 nm).

3. Results

3.1 Ni-Based Resistors

Table 3 shows the sheet resistance R_{sh} (i.e., the resistance R divided by the number of squares given by the ratio length/width) of as-sprayed Ni-based resistors. These data are not intended for a *straight* comparison between R_{sh} values of different sample series: The sheet resistance is not normalized to one specific thickness, and the actual thickness of the resistors differs in the various series. Instead, we wish to focus on the standard deviations, which indicate the reproducibility of the sheet resistance for samples prepared by the same laboratory. The most relevant difference in samples prepared by the various suppliers concerns the effect of annealing which was studied with repeated heating ramps and isothermal processes at various temperatures. Figure 3 shows the resistance measured at room temperature for a Z-Ni resistor submitted to annealing processes lasting 2 h at various temperatures (see Section 2). It is apparent that the annealing results in a resistance decrease, beginning at temperatures as low as $200\text{--}250\text{ }^{\circ}\text{C}$ and completed at about $350\text{ }^{\circ}\text{C}$. The same effect (an irreversible decrease of resistance in heated samples) was observed after the first heating cycle, as shown in Fig. 4. This figure displays the resistance as a function of temperature for a Z-Ni sample during the first and second heating ramps. The curves overlap at a temperature of around $350\text{ }^{\circ}\text{C}$, indicating that the effect of annealing is completed at this temperature.

Table 3 Mean sheet resistance R_{sh} and its standard deviation for as-sprayed and annealed Ni-based resistors

Sample series	R_{sh} , $\text{m}\Omega/\text{sq}$		Resistivity, ρ , $\mu\Omega\text{ cm}$	Mean thickness, μm
	As-sprayed	As-annealed		
R-Ni	8.8 ± 0.8	7.1 ± 0.7	26.7 ± 16.7	38 ± 18
Z-Ni	6.3 ± 0.15	5.6 ± 1.0	34.6 ± 11.2	62 ± 9
F-Ni	156.9 ± 0.03	94.8 ± 12.3	(a)	15 ± 10

(a) Too irregular thickness and pinching of the patterns

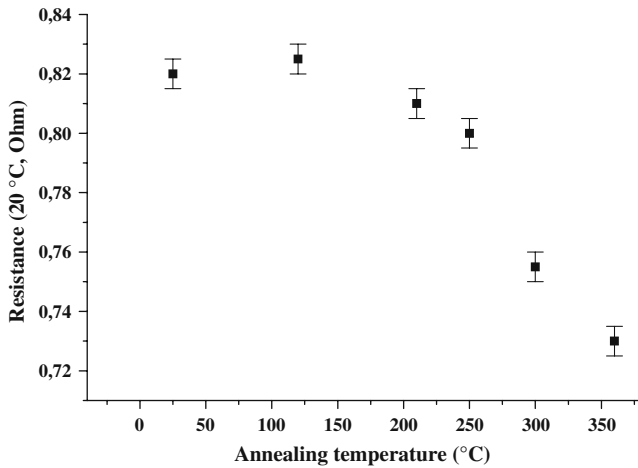


Fig. 3 Resistance of sample Z-Ni, measured at room temperature after 2 h lasting isotherm annealing at various temperatures T (see Section 2 for details)

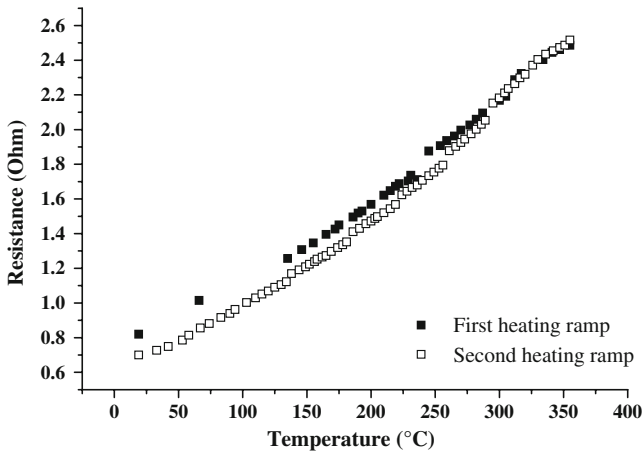


Fig. 4 Resistance as a function of temperature for Z-Ni samples showing a decrease in resistance after the first heating ramp. The heating rate was approximately 6 °C/min

No further change of resistance or its temperature dependence was observed even after tens of heating cycles and long time dwelling (500 h) at temperatures as high as 600 °C (Ref 8). Similar experiments were carried out for the R-Ni and F-Ni samples. The results show an irreversible change of $\Delta R/R = -42 \pm 4\%$ in F-Ni samples but much lower in R-Ni and Z-Ni samples (Table 3).

The “final” sheet resistance reported in Table 3 represents that irreversible value was observed after annealing. Likewise, the resistivity given in Table 3 is the value computed from these ultimate resistances. It should be noted that the major contribution to the uncertainty in resistivity evaluations is the irregular thickness of the resistors, as will be discussed in Section 4. Nevertheless, the evaluated resistivity is comparable to that reported by Pawlak (Ref 14) but notably lower than that measured by Younis et al. (Ref 7).

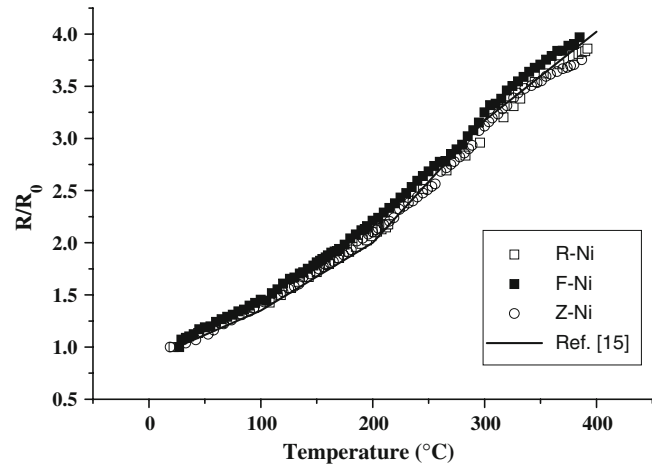


Fig. 5 Relative resistance as a function of temperature for Ni samples prepared in three different laboratories. The error bars are within symbols. Literature data is included for comparison

Despite the different behaviors (in terms of relative change of resistance after annealing) of samples prepared in different laboratories, the resistance of all the Ni-based resistors exhibited the same temperature dependence. Figure 5 shows the normalized resistance $R(T)/R(20\text{ °C})$ as a function of temperature for representative samples from each series of Ni-based resistors. The curves overlap and, in addition, replicate the behavior predicted for pure bulk Ni (e.g., sheet and wires (Ref 15)), including its characteristic “kink” at the Curie temperature ($\sim 350\text{ °C}$).

These results are far from an obvious expectation as thermally sprayed nickel coatings contain impurity phases. In fact, due to the high affinity of Ni to oxygen and the very high temperatures reached in the plasma plume, the presence of oxidized material is unavoidable in APS-sprayed Ni coatings (Ref 16-18). According to SEM-EDS analyses, the oxide is mainly confined in isolated regions, appearing like “islands”, in an almost homogenous surrounding matrix (Fig. 6). An evaluation of the amount of incorporated oxygen was done by means of semi-quantitative EDS analyses, image analyses of BSE pictures, and visual inspection of the relative intensity of XRPD peaks. The data revealed different amounts of incorporated oxygen in samples of the various series. For example, R-Ni sample are more oxidized than F-Ni resistors: EDS analyses show in the former samples a relative amount of detected oxygen in the range from 11.3 wt.% (spectrum 1 in Fig. 6a) to 1.0 wt.% (spectrum 2 in Fig. 6a) while in F-Ni samples no more than 1 wt.% of oxygen was detected in any part of the resistor. Less frequent is the presence of pores, e.g., in F-Ni samples (Fig. 6b) while the R-Ni samples are essentially compact. It is remarkable that no variation in the microstructural features of as-sprayed and annealed samples could be detected either with SEM-EDS analyses. These observations indicate that the different response to annealing processes cannot be interpreted by the consideration of details like porosity and oxide volume alone. This will be addressed later in Section 4.

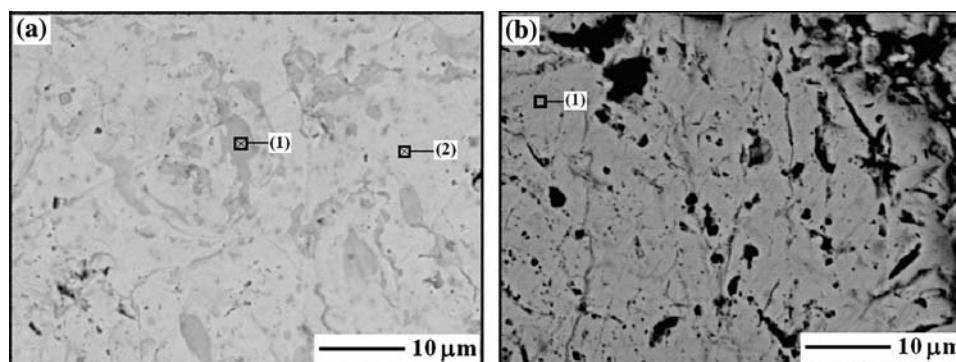


Fig. 6 In-plane view BSE-images of Ni-based samples from the series R-Ni (a) and F-Ni (b). The samples were gently polished prior to analyses. The gray regions make evident oxidized material. Points where EDS analyses were performed are numerated (see text for details). Missing solid matter appears as black areas

Table 4 Mean sheet resistance R_{sh} of as-sprayed Ni20Cr resistors

Sample series	R_{sh} , mΩ/sq	t , μm	ρ , μΩ cm	TCR, ppm/°C
R-Ni20Cr	205	50 ±	411 ± 100	218
Z-Ni20Cr	122	38 ± 12	463 ± 146	184
P2-Ni20Cr	78.5	36 ± 4	283 ± 80	870
F-Ni20Cr	322 ± 40	12 ± 3	386 ± 144	224
S-Ni20Cr	166.4	22 ± 5	366 ± 126	1064
P1-Ni20Cr	57.0	26 ± 9	217 ± 77	1331
S-Ni20Cr-HVOF	76.3	24 ± 17	183 ± 149	2833

Resistor thickness t , computed resistivity ρ , and measured TCR are also reported

3.2 Ni20Cr-Based Resistors

Table 4 reports the mean sheet resistance of as-sprayed resistors prepared with Ni20Cr powders, together with resistor thickness, temperature coefficient of resistance, and calculated resistivity. The relative spread of resistance values in a given series is acceptable (from a few percent to 20%). As in the case of Ni-resistors (see previous section), the major contribution to the low precision in resistivity evaluation comes from the variations in the thickness profiles. Nevertheless, it is observed that the mean resistivity values are in the range of 300-400 μΩ cm as found by other researchers (Ref 6).

A small relative change of resistance due to annealing at temperatures higher than 400 °C is observed in Ni20Cr resistors. Opposite to Ni-resistors (see Section 3.1), annealing results in a *positive* relative change of resistance. This effect is shown in Fig. 7 which compares the R vs. T curves for the first heating ramp of an as-sprayed Z-Ni20Cr sample and its second heating ramp. The resistance at room temperature increased with 3.9%. No more shift of the resistance value was observed in subsequent annealing processes. Heating at higher temperatures than 300 °C was generally not carried out because of the risk of failures in these Ni20Cr-based resistors (Ref 13). The most relevant difference in Ni20Cr-resistors prepared in various laboratories concerns the TCR values, as shown in Table 4 and Fig. 8. The TCR spans from 184 ppm/°C (close to the TCR of nichrome (Ref 19)) to 1330 ppm/°C for

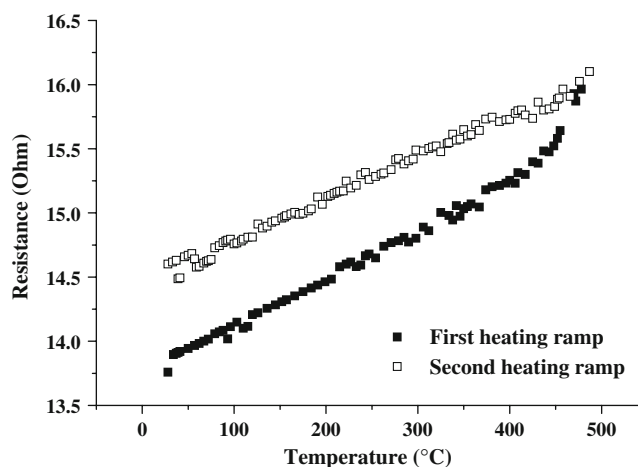


Fig. 7 Resistance as a function of temperature for a sample Z-Ni20Cr. The as-prepared sample was heated to 478 °C (first heating ramp), held at that temperature for ca. 3 h, cooled down to room temperature and again heated (second heating ramp) up to 487 °C

APS-sprayed resistors while a TCR of 2830 ppm/°C was found for HVOF-sprayed samples.

Analytical investigations provided important data for the interpretation of these results. Figure 9 shows representative BSE images of Ni20Cr-based samples investigated in this study. Gray regions, rich in oxygen, in a

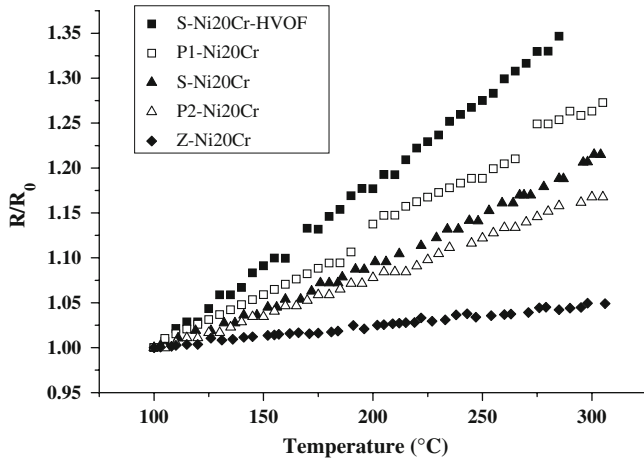


Fig. 8 Relative resistance as a function of temperature for Ni20Cr-based resistors prepared in different laboratories

brighter surrounding matrix are observed in the majority of the samples (Fig. 9). Exceptions are images of samples R-Ni20Cr and F-Ni20Cr, which show an almost uniform contrast. The results of EDS analyses performed on extended regions of the samples surfaces are shown in Table 5. The data show, not surprisingly, a significant uptake of oxygen in the sprayed material. The relative oxygen concentration, ranging from about 1.5% to 10%, is in fact notably higher than that in the powders (<0.1%, Table 2). Air engulfment by the plasma jet in APS, preferential oxidation of Cr and postimpact oxidation of the splats, are all responsible for this uptake as shown by detailed investigations of Ni-bearing alloys, either Ni20Cr (Ref 20, 21) or NiAl (Ref 22) as well as of NiCrAlY (Ref 23, 24). The large variation of oxygen content in samples prepared by different laboratories evidences the complex interrelationship between oxidation and process parameters (e.g., particle temperature, particle velocity, standoff distance, shrouding atmosphere). However, the

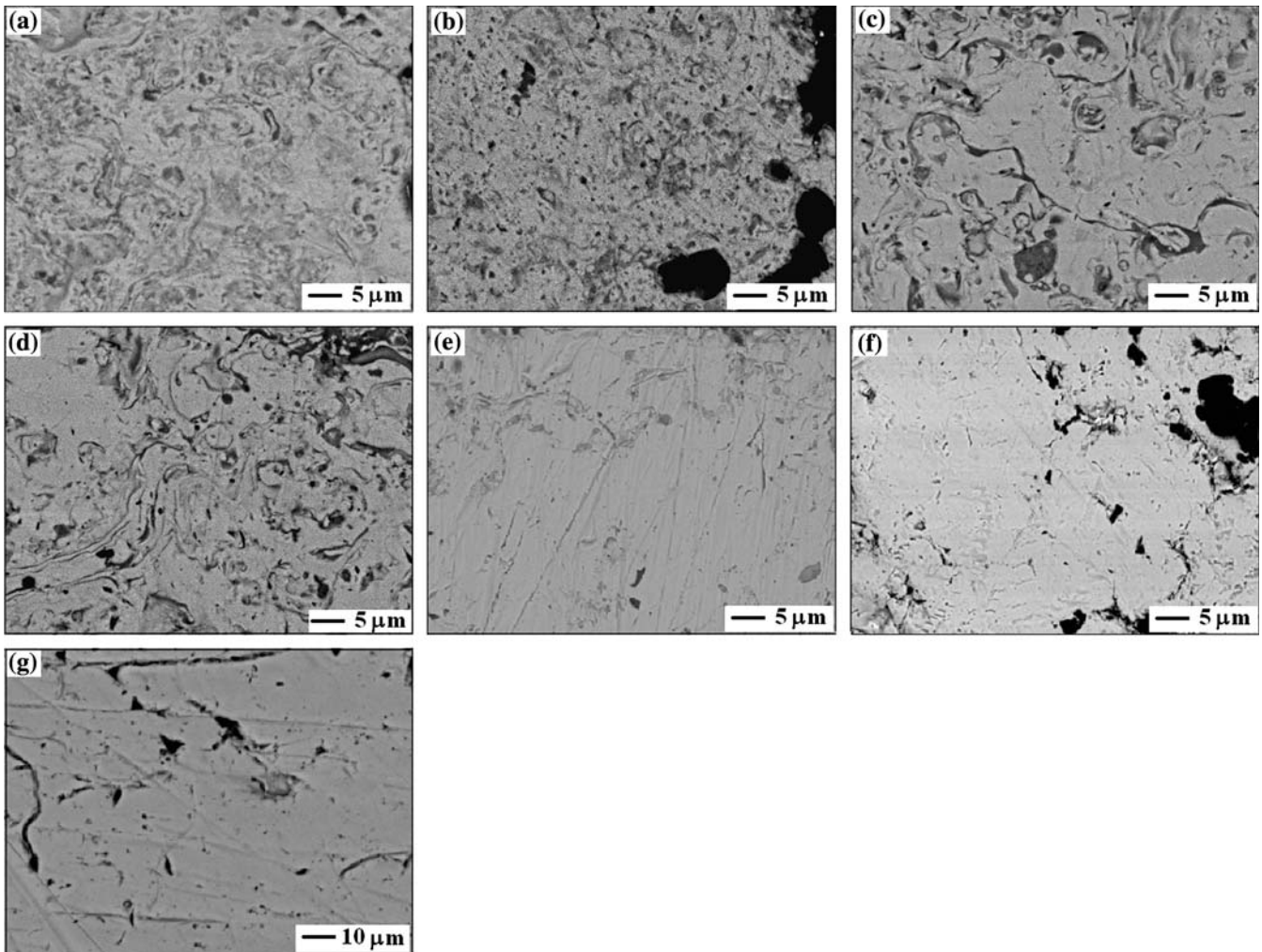


Fig. 9 In-plane view BSE-images of Ni20Cr samples from the series R-Ni20Cr-HVOF (a), S-Ni20Cr (b), P1-Ni20Cr (c), P2-Ni20Cr (d), Z-Ni20Cr (e), F-Ni20Cr (f), and R-Ni20Cr (g). Results of EDS analyses on extended areas are reported in Table 5

particle size appears the dominant factor in our study because of the strict correlation between the oxygen content and the size of the original powders (compare Table 5 with Table 1). This correlation may be expected because of the larger surface areas offered by finer particles to physico-chemical surface reactions in the high plume temperature. This generally expected reactivity has been experimentally determined in case of HVOF-sprayed MCrAlY powders by Li and Li (Ref 23). In addition, data in Table 5 show that the Ni/Cr ratio, when measured on an extended area of the film (e.g., $15 \times 15 \mu\text{m}^2$), does not notably deviate from that (4.0 ± 0.25) of the original powders. Hence, no

preferential evaporation of Cr (generally the most volatile of the powder constituents) was observed. However, the Ni/Cr ratio detected in the darker areas of Fig. 9 (the oxidized material) is consistently lower than that measured in the surrounding matrix. These results indicate that oxidation results in depletion of Cr in the metal matrix, which composition thus changes from 80Ni20Cr to $x\text{Ni}y\text{Cr}$ with $x/y > 4$, and an enrichment of Cr in the new phases formed in the spray process.

Figure 10 shows a BSE image and the corresponding elemental maps for a cross-sectional area of a representative resistor from the series S-Ni20Cr. Severe segregation can be observed. The oxygen-rich areas contain Cr

Table 5 Elemental composition determined by EDS analysis of Ni20Cr-samples prepared by different facilities (analyzed area: $70 \times 80 \mu\text{m}^2$)

Sample	Elemental composition, wt.%					
	O	Si	Cr	Mn	Fe	Ni
S-Ni20Cr-HVOF	9.4 ± 0.5	1.0 ± 0.1	16.6 ± 0.3	73.1 ± 0.5
S-Ni20Cr	8.5 ± 0.5	1.9 ± 0.2	17.5 ± 0.3	72.0 ± 0.5
P1-Ni20Cr	6.5 ± 0.4	0.4 ± 0.1	19.9 ± 0.3	73.1 ± 0.5
P2-Ni20Cr	5.7 ± 0.5	0.4 ± 0.1	19.7 ± 0.3	74.2 ± 0.5
Z-Ni20Cr	3.7 ± 0.3	1.4 ± 0.1	19.7 ± 0.2	...	0.4 ± 0.1	74.8 ± 0.3
F-Ni20Cr	...	1.2 ± 0.1	20.2 ± 0.2	...	0.3 ± 0.1	73.4 ± 0.2
R-Ni20Cr	1.5 ± 0.1	1.7 ± 0.1	19.2 ± 0.1	0.8 ± 0.1	0.1 ± 0.05	76.6 ± 0.2

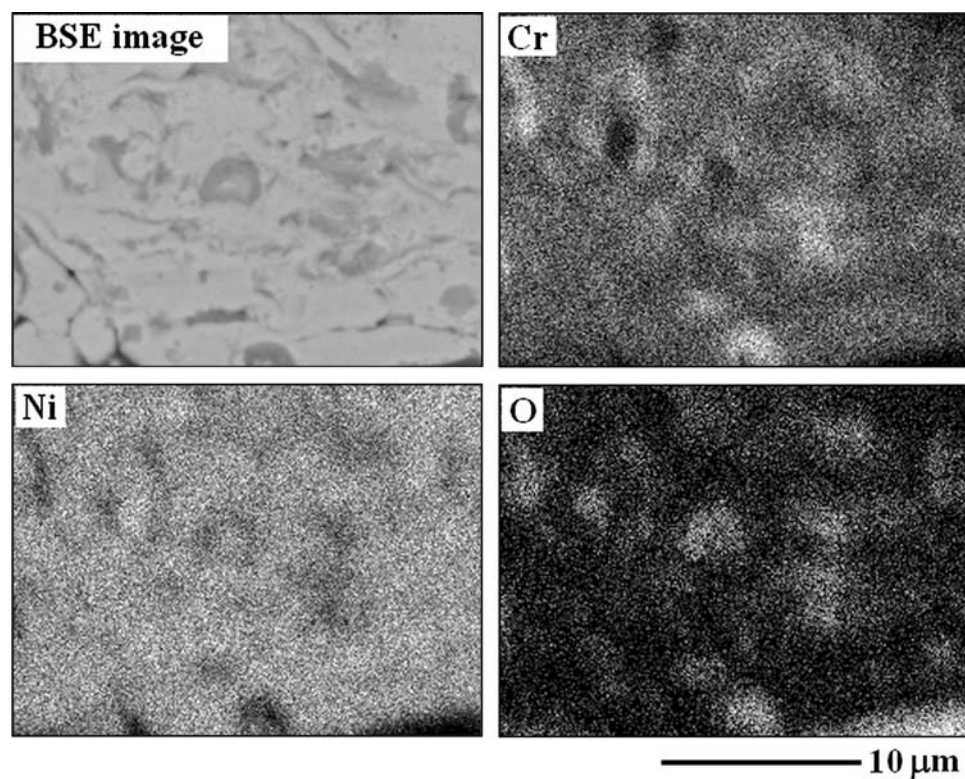


Fig. 10 BSE image and elemental maps of a cross-sectional area of sample S-Ni20Cr, showing segregation of the metals as well as severe oxidation. Note that oxygen-rich areas contain Cr but are depleted of Ni. This enrichment of Cr in the oxidized areas leads to a depletion of Cr and enrichment of Ni in the surrounding matrix

but are depleted of Ni. This enrichment in Cr in the oxidized areas leads to depletion of Cr and enrichment of Ni in the surrounding areas.

Figure 11 displays the XRPD patterns collected from samples of the series R-Ni20Cr (a) and S-Ni20Cr-HVOF (b). The most intense peaks are assigned to the NiCr alloy. Due to the relatively thin metal layer (30–40 μm), peaks from the underlying alumina layer appears in the pattern collected from S-Ni20Cr-HVOF. No metal oxide phases could be detected in the R-Ni20Cr sample, whereas peaks assigned to NiCr_2O_4 were observed in S-Ni20Cr-HVOF samples (JCPDS card 00-023-1271). However, the presence of NiO_x in the latter sample is quite probable but not detectable in the XRPD pattern, as the major peaks of this phase overlap with the intense peaks of NiCr_2O_4 .

XRPD patterns of F-Ni20Cr, Z-Ni20Cr, and R-Ni20Cr (only the latter one reported in Fig. 11 for clarity) showed only peaks assigned to a NiCr alloy. These findings support the results from the EDS analyses, which showed a low amount of oxidized material in these samples (see Fig. 9).

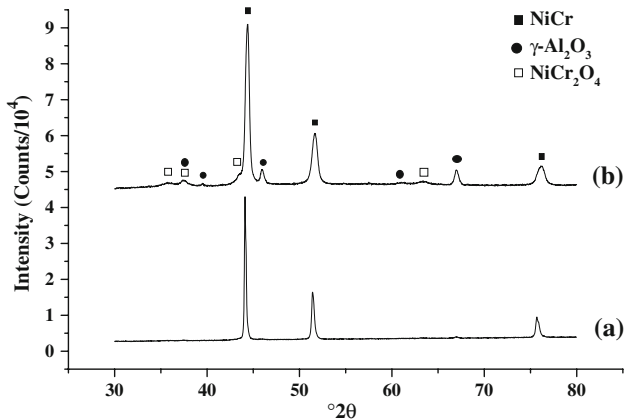


Fig. 11 XRPD patterns collected from samples of the series (a) R-Ni20Cr and (b) S-Ni20Cr-HVOF

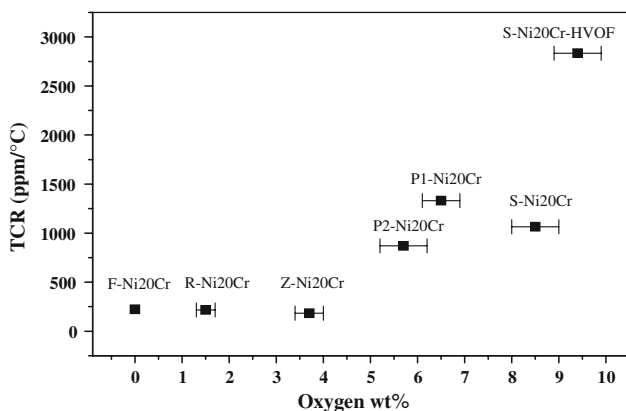


Fig. 12 Temperature coefficient of resistance (TCR) as a function of oxygen content as determined by EDS analyses in Ni20Cr-based resistors

Finally, Fig. 12 plots the TCR values as a function of the oxygen content in the different samples. A clear correlation is observed between these quantities. The TCR value of the resistor increases with oxygen content.

4. Discussion

Relationships between processing, microstructure, and properties are the foundation on which materials science is built on. A search for such relationships is made particularly hard in the case of thermally sprayed materials because of the myriad of parameters which define their microstructure (Ref 1-3). Therefore, it is not surprising that different functional properties are observed in coatings prepared in various laboratories. In fact, astonishing different electrical properties in terms of resistivity and reliability (stability vs. failure modes) have been experienced in MIT Laboratories while studying materials apparently prepared with the same procedures (Ref 6, 7), and in terms of resistivity of Ni materials prepared by different thermal processes (Ref 11). In this work, we have collected further data on the correlation between microstructure and electrical properties of APS- and HVOF-sprayed metals.

4.1 Nickel

The relevant features observed in Ni-based resistors are summarized in the following points:

- The resistivity of our annealed samples is consistent with data reported by other authors, taking into account the poor definition in the shape and size of the resistors.
- After annealing an irreversible change of resistance occurs, which leads in some cases to a relative negative change of resistance larger than 40%.
- Despite evident differences in microstructure (extent of oxidized material in the matrix, porosity), Ni-based resistors exhibit the same temperature dependence of resistance.

To our knowledge, the finding of point (b) was never reported before for thermal-sprayed electrical conductors, but only for thin films (Ref 25-27) and bulk materials (Ref 28). The effect has been interpreted as being connected to various physical phenomena. In thin films, a resistivity decrease may be related to re-crystallization and grain growth of the very fine (and therefore very “reactive”) original agglomerates of atoms which nucleate on the substrate (Ref 25). These effects should be negligible in thermal-sprayed metals whose splats are quite larger and thicker than thin films. However, also annealing of film defects formed during deposition has been advocated (Ref 27). In massive materials, on the other hand, it has been shown since a long time that annealing removes structural defects such as extra vacancies and dislocations present in quenched materials (Ref 28). As a consequence, the recovery of the electrical resistivity to its fully annealed value has been extensively studied and found to be a

powerful method for studying defect removal from the structure by annealing (Ref 28). Microstructural defects are certainly present in thermal-sprayed metals, as witnessed by the high levels of mechanical stresses measured in APS and HVOF coatings (Ref 29-31). One possible origin of the irreversible decrease of resistivity observed in Ni-based resistors is the recovery of polygonized cells observed in APS nickel by Sampath and Hermann (Ref 18). Thus, a possible interpretation of the different amount of recovery in resistance after annealing in resistors prepared in different laboratories (and in resistors prepared with the same processes on different substrates) may be interpreted in terms of different process parameters leading to different defect density in the as-sprayed materials to be annealed out by thermal energy.

Transmission electron microscopy (TEM) investigations could better elucidate our results and evidence a possible correlation with the dislocations structure and distribution in Ni-layers. In this scenario, the comparison between the resistivity of as-sprayed and annealed layers might be a simple method for evaluating the effect of deposition parameters on physical properties of coatings, including the residual stress.

Turning back to the temperature dependence of the normalized resistance, the noted consistent behavior in all investigated samples, notwithstanding their different amount of oxidized regions and porosity, may be interpreted in the following way: The regions of Ni-oxides (which notoriously exhibit high resistivity) and the pores as well, subtract conductive material to electrical transport, forcing the current to percolate through the more conductive undisturbed Ni-matrix. Therefore, the TCR values are dominated by the electrical properties of the “pure” Ni material.

4.2 Ni20Cr

The relevant findings for Ni20Cr-based resistors are summarized in the following points:

- (d) The mean resistivity, even though roughly evaluated, is comparable with that quoted by other authors.
- (e) A minor effect of annealing on resistivity has been observed.
- (f) Large differences in the R vs. T curves were observed, with TCR values intimately related to amount of oxygen incorporated in the material. The oxide formation results in a change of the alloy composition which becomes richer in Ni compared to the 80/20 original powder.

The finding summarized in point (e), i.e., the small increase in resistance after annealing of some Ni20Cr samples (see Table 3 and Fig. 11) is probably a consequence of ordering of atoms in the alloy, a phenomenon previously observed in NiCr alloy annealed at 800 °C and slowly cooled down to room temperature (Ref 32).

The finding summarized in point (f) can be interpreted with the following considerations: The TCR of

bulk NiCr alloys is notably dependent on the Ni/Cr ratio, being higher for higher Ni/Cr ratio (Ref 32). The Ni/Cr ratio in sprayed NiCr materials is effected by the extent of oxidation as this phenomenon results in the depletion of Cr in the metal alloy. Our results show evidence of these effects, especially when finer powders were used and when metal deposition was performed with HVOF. Therefore, the sequence of events and their consequences can be traced as follows: Fine powders or oxygen-rich atmosphere in the plume lead to the formation of oxide phases (mainly chromite, i.e., NiCr₂O₄ and NiO), which are notoriously highly resistive materials (Ref 33, 34). This situation implies that the electrical transport is forced in the surrounding metal matrix, which has a higher Ni/Cr ratio compared to the feedstock powder (80Ni20Cr alloy). Consequently, the TCR values in these materials are higher. This interpretation is consistent with the strict correlation noted between oxygen concentration and powder size (compare Table 5 with Table 1) and between oxygen content and TCR (see Fig. 12). Hence, to achieve low and reproducible TCR values the following strategies could be useful: the choice of coarse Ni20Cr feedstock powders and a strict control of the oxidation conditions, or feedstock powders richer in Cr than 20% provided that reproducible spray conditions are known for the transformation in the Ni20Cr desired final composition.

5. Conclusions

Electrical properties of resistors prepared with Ni and Ni20Cr powders by thermal spray processes (APS and HVOF) were studied. It was found that the resistivity of Ni resistors decreased after annealing at temperatures in the range 200-400 °C. It was suggested that this phenomenon could be related to healing of structural defects. On the contrary, the observed increase of resistivity of Ni20Cr-based resistors is possibly due to ordering of the atoms. The temperature dependence of resistance for Ni-based resistors was invariably the same as for Ni bulk, regardless of sample origin. On the other hand, a large spread in TCR values of Ni20Cr-based resistors were observed. These results were attributed to different amounts of oxide phases in the samples. A clear correlation was found between the oxygen content in the resistors and the TCR values. This was explained by the increased Ni/Cr ratio in the resistor matrix, due to preferential oxidation of Cr in the high temperature flames of APS and HVOF processes.

Therefore, it turns out that the electrical properties of resistors may provide significant insights to the microstructure of sprayed metals. The temperature coefficient of resistance of NiCr coatings is sensitive to newly formed phases, whereas the relative change of resistance after annealing of Ni-based coatings may be an indicator of residual stresses in the sprayed metal.

Finally, we note that the high temperature coefficient of resistance (6000–7000 ppm/°C), the reproducibility of R

vs. T curves, and the long-time stability of APS Ni-based resistors render them excellent candidates for temperature sensors and self-controlled high temperature heaters.

Acknowledgments

The authors are grateful to Centro Sviluppo Materiali (CSM), Rome, Italy for financially supporting this project. We are also indebted to INGLASS S.r.l, San Polo di Piave, Treviso, Italy, for having promoted this research.

References

- L. Pawłowski, *The Science and Engineering of Thermal Spray Coatings*. Wiley, Chichester, 1995
- R. McPherson, *Plasma-Sprayed Ceramic Coatings*, *Surface Engineering: Processes and Applications*, K.N. Strafford et al., Eds., Technomic Publications, 1995, p 3-20
- A. Sharma, R.J. Gambino, and S. Sampath, Anisotropic Electrical Properties in Thermal Spray Metallic Coatings, *Acta Mater.*, 2006, **54**, p 59-65
- R. Gadow, A. Killinger, and C. Li, Product Development with Thermally Sprayed Functional Coatings on Glass and Glass-Ceramics Substrates, *Int. J. Appl. Ceram. Technol.*, 2005, **2**, p 493-503
- T. Tong, J. Li, Q. Chen, J.P. Longtin, S. Tankiewicz, and S. Sampath, Ultrafast Laser Micromachining of Thermal Sprayed Coatings for Microheaters: Design, Fabrication and Characterization, *Sens. Actuators A*, 2004, **114**, p 102-111
- D. Michels, J. Hadel, and J.H.V. Lienhard, High Heat Flux Resistance Heaters from VPS and HVOF Thermal Spraying, *Exp. Heat Transfer*, 1998, **11**, p 341-359
- H.F. Younis, R.S. Dahbura, and J.H.V. Lienhard, Thin Film Resistance Heaters for High Heat Flux Jet Array Cooling Experiments, *Proc. ASME Heat Transfer Division 3*, ASME HTD, 1997, **353**, p 127-134
- M. Prudenziati, G. Cirri, and P. Dal Bo, Novel High-Temperature Reliable Heaters in Plasma Spray Technology, *J. Therm. Spray Technol.*, 2006, **15**, p 329-331
- J. Longtin, S. Sampath, R.J. Gambino, S. Tankiewicz, and R. Greenlaw, Sensors for Harsh Environments by Direct Write Thermal Spray, *IEEE Sens. J.*, 2004, **4**, p 118-121
- R.J. Gambino, M. Manivel Raja, S. Sampath, and R. Greenlaw, Plasma Sprayed Thick Film Anisotropic Magnetoresistive (AMR) Sensors, *IEEE Sens. J.*, 2004, **4**, p 764-767
- N. Margadant, S. Siegmann, J. Patscheider, T. Keller, W. Wagner, J. Ilavsky, J. Pisacka, G. Barbexat, and P. Fiala, Microstructure-Property Relationship And Cross-Property Correlations of Thermal Sprayed Ni-Alloy Coatings, *Proc. Thermal Spray 2001: New Surfaces for a New Millennium*, C.C. Berndt, K.A. Khor, and E.F. Lugscheider, Eds., ASM International, Materials Park, OH, 2001, p 643-652
- S. Sampath, H. Herman, A. Patel, R. Gambino, R. Greenlaw, and E. Tormey, Thermal Spray Techniques for Fabrication of Meso-Electronics and Sensors, *Material Research Society Symposium Proceedings*, 2000, **624**, p 181-188
- M. Prudenziati, Development and the Implementation of High-Temperature Reliable Heaters in Plasma Spray Technology, *J. Therm. Spray Technol.*, 2008, **17**, p 234-243
- R. Pawlak, Laser-Remelted Plasma Coatings, *Proc. SPIE—The International Society for Optical Engineering. Laser Technology VII: Applications of Lasers*, 2003, **5229**, p 251-254
- E.P. Wolfarth, *Ferrimagnetic Materials*, North Holland, 1980
- H. Herman, S. Sampath, and R. McCune, Thermal Spray: Current Status and Future Trends, *MRS Bull.*, 2000, **25**, p 17-25
- R. McPherson, The Relationship Between the Mechanism of Formation, Microstructure and Properties of Plasma-Sprayed Coatings, *Thin Solid Films*, 1981, **83**, p 297-310
- S. Sampath and H. Herman, Rapid Solidification and Microstructure Development During Plasma Spray Deposition, *J. Therm. Spray Technol.*, 1996, **5**(4), p 445-456
- R.A. Serway, *Principles of Physics*, (2nd ed.). Saunders College Pub. London, Fort Worth, TX, 1998
- P. Chráska, B. Kolman, M. Suchánek, and K. Voleník, Composition Changes of Selected Alloys During Their Plasma Spraying, *Thermal Spray 2004: Advances in Technology and Application, Proceedings of the International Thermal Spray Conference*, May 10-12, 2004 (Osaka, Japan), 2004, p 7-11
- K. Voleník, P. Chráska, and J. Dubský, Oxidation of Ni-Based Alloys Sprayed by a Water-Stabilized Plasma Gun (WSP®), *Proc. of the ITSC 2003: Advancing the Science & Applying the Technology* (Orlando, OH), C. Moreau and B. Marple, Eds., ASM International, Materials Park, OH, 2003, p 1033-1040
- K. Volenik, B. Kolman, J. Dubsky, and P. Chraska, In-Flight Behaviour of Ni-Al Powder During Its Plasma Spraying, *Proceedings of the ITSC 2005—Thermal Spray Connects: Explore its Surfacing Potential!* May 2-4, 2005 (Basel, Switzerland), 2005, p 1175-1178
- C.-J. Li and W.-Y. Li, Effect of Sprayed Powder Particle Size on the Oxidation Behavior of MCrAlY Materials During High Velocity Oxygen-Fuel Deposition, *Surf. Coat. Technol.*, 2002, **162**, p 31-41
- V.V. Sobolev and J.M. Guilemany, Oxidation of Coatings in Thermal Spraying, *Mater. Lett.*, 1998, **37**, p 231-235
- J.L. Vossion and W. Kern, *Thin Films Processes*. Academic Press, New York, 1987
- I.H. Kazi, P.M. Wild, T.N. Moore, and M. Sayer, The Electro-mechanical Behavior of Nichrome (80/20 wt.%) Film, *Thin Solid Films*, 2003, **433**, p 337-343
- M.M. Nayak, R. Rajanna, and S. Mohan, Performance Study of a Pressure Transducer with Meandering-Path Thin Film Strain Gauges, *Thin Solid Films*, 1990, **193/194**, p 1023-1029
- R.W. Cahn and P. Haasen, *Physical Metallurgy*, 3rd ed., part II, Elsevier Sci. Publ., Amsterdam, 1983
- S. Kuroda and T.W. Clyne, The Quenching Stress in Thermally Sprayed Coatings, *Thin Solid Films*, 1991, **200**, p 49-66
- T. Keller, N. Margadant, T. Pirling, M.J. Riegert-Escribano, and W. Wagner, Residual Stress Determination in Thermally Sprayed Metallic Deposits by Neutron Diffraction, *Mater. Sci. Eng. A*, 2004, **373**, p 33-44
- S. Sampath, X.Y. Jiang, J. Matejcek, L. Prchlik, A. Kulkarni, and A. Vaidya, Role of Thermal Spray Processing Method on the Microstructure, Residual Stress and Properties of Coatings: An Integrated Study for Ni-5 wt.%Al Bond Coats, *Mater. Sci. Eng. A*, 2004, **364**, p 216-231
- K. Schröder, *Handbook of Electrical Resistivities of Binary Metallic Alloys*. CRC Press, Florida, 1983, p 194-197
- E.J. Verwey, P.W. Haayman, and F.C. Romeijn, Physical Properties and Cation Arrangement of Oxides with Spinel Structures, *J. Chem. Phys.*, 1947, **15**, p 181-187
- W.D. Kingery, D.R. Uhlman, and H.K. Bowen, *Introduction to Ceramics*. Wiley Interscience, New York, 1975